J|A|C|S
ARTICLES
Published on Web 06/15/2005

Imidazole-Based Excited-State Intramolecular Proton-Transfer Materials: Synthesis and Amplified Spontaneous Emission from a Large Single Crystal

Sanghyuk Park,[†] Oh-Hoon Kwon,[‡] Sehoon Kim,[†] Sangwoo Park,[§] Moon-Gun Choi,[§] Myoungsik Cha,[⊥] Soo Young Park,*[,†] and Du-Jeon Jang*[,‡]

Contribution from the School of Materials Science and Engineering, Seoul National University, ENG 445, Seoul 151-744, Korea, School of Chemistry, Seoul National University, NS60, Seoul 151-742, Korea, Center for Bioactive Molecular Hybrids, Yonsei University, Seoul 120-749, Korea, and Department of Physics, Pusan National University, Pusan 609-735, Korea

Received February 9, 2005; E-mail: parksy@snu.ac.kr; djjang@snu.ac.kr

Abstract: We have synthesized a novel class of imidazole-based excited-state intramolecular proton-transfer (ESIPT) materials, i.e., hydroxy-substituted tetraphenylimidazole (HPI) and its derivative HPI-Ac, which formed large single crystals exhibiting intense blue fluorescence and amplified spontaneous emission (ASE). Transparent, clear, and well-defined fluorescent single crystals of HPI-Ac as large as 20 mm × 25 mm × 5 mm were easily grown from its dilute solution. From the X-ray crystallographic analysis and semiempirical molecular orbital calculation, it was deduced that the four phenyl groups substituted into the imidazole ring of HPI and HPI-Ac allowed the crystals free from concentration quenching of fluorescence by limiting the excessive tight-stacking responsible for intermolecular vibrational coupling and relevant nonradiative relaxation. Fluorescence spectral narrowing and efficient ASE were observed in the HPI-Ac single crystal even at low excitation levels attributed to the intrinsic four-level ESIPT photocycle.

Introduction

Highly fluorescent organic materials including molecular laser dyes and conjugated polymers have been extensively investigated as the active gain media for optically pumped solid-state lasers.[1] Different from the various classes of fluorescent dyes investigated so far, the one based on excited-state intramolecular proton transfer (ESIPT) has an intrinsic advantage for stimulated emission because it is harnessed with a favorable four-level photophysical cycle.[2] The ESIPT reaction, a fast enol (E)-to-keto (K) prototropy occurring in the excited states of intramolecularly H-bonded molecules, is thus gaining ever increasing interest due to the fundamental importance of the peculiar photophysical processes as well as the potential applications to the laser dyes,[3−6] solar energy concentrators,[7] chemosensors,[8] and electroluminescent materials.[9] Because the ESIPT molecules

Scheme 1. Schematic Representation of ESIPT Photocycle

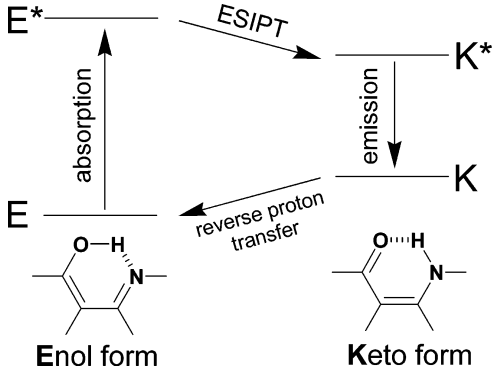

are normally more stable in E forms in the ground states but in K* forms in the excited states, photoexcitation of them is immediately followed by the four-level cyclic proton-transfer reactions (E→E*→K*→K→E) mediated by the intramolecular H-bonds (Scheme 1).[2] It is characteristically observed, therefore, that the absorption from E and emission from K* results in an abnormally large Stokes shift with no self-absorption, providing an ideal scheme for the proton-transfer lasers[3−6] and UV-photostabilizers.[10]

To realize a compact and rugged device of high performance, most of the ESIPT applications demand highly dense solid-state

[†] School of Materials Science and Engineering, Seoul National University.
[‡] School of Chemistry, Seoul National University.
[§] Center for Bioactive Molecular Hybrids, Yonsei University.
[⊥] Department of Physics, Pusan National University.

(1) Tessler, N. *Adv. Mater.* **1999**, *11*, 363.
(2) (a) Weller, A. *Z. Elektrochem.* **1956**, *60*, 1144. (b) Weller, A. *Prog. React. Kinet.* **1961**, *1*, 188. (c) Sengupta, P. K.; Kasha, M. *Chem. Phys. Lett.* **1979**, *68*, 382.
(3) (a) Kasha, M. *J. Chem. Soc., Faraday Trans. 2* **1986**, *82*, 2379. (b) Gormin, D.; Sytnik, A.; Kasha, M. *J. Phys. Chem. A* **1997**, *101*, 672. (c) Chou, P.; McMorrow, D.; Aartsma, T. J.; Kasha, M. *J. Phys. Chem.* **1984**, *88*, 4596.
(4) Sastre, R.; Costela A. *Adv. Mater.* **1995**, *7*, 198.
(5) Tarkka, R. M.; Zhang, X.; Jenekhe, S. A. *J. Am. Chem. Soc.* **1996**, *118*, 9438.
(6) Costela, A.; Garcia-Moreno, I.; Mallavia, R.; Amat-Guerri, F.; Barroso, J.; Sastre, R. *Opt. Commun.* **1998**, *152*, 89.
(7) Volmer, F.; Rettig, W. *J. Photochem. Photobiol. A: Chem.* **1996**, *95*, 143.
(8) Shynkar, V. V.; Klymchenko, A. S.; Piemont, E.; Demchenko, A. P.; Mely, Y. *J. Phys. Chem. A* **2004**, *108*, 8151.
(9) (a) Ma, D.; Liang, F.; Wang, L.; Lee, S. T.; Hung, L. S. *Chem. Phys. Lett.* **2002**, *358*, 24. (b) Osaheni, J. A.; Jenekhe, S. A. *J. Am. Chem. Soc.* **1995**, *117*, 7389.
(10) Luiz, M.; Biasutti, A.; Soltermann, A. T.; Garcia, N. A. *Polym. Degrad. Stab.* **1999**, *63*, 447.

10.1021/ja0508727 CCC: $30.25

Scheme 2. Synthetic Routes to the Hydroxy-Substituted Tetraphenyl Imidazole (HPI), Methyl-Blocked HPI (MeOPI), and Acetate-Containing Derivative (HPI-Ac)

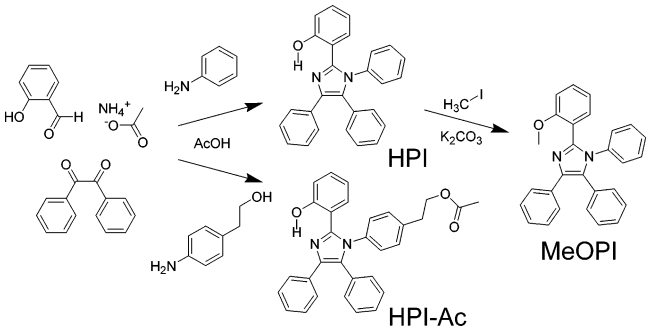

systems. However, the intermolecular interactions in the condensed phase are often associated with the problem of significant concentration quenching in the fluorescence intensity, which is a serious challenge in the fluorescent ESIPT materials as well. Recently, we have demonstrated that site-isolation by dendritic architecture[11,12] or specific J-aggregation with favorable intermolecular interaction[13] could effectively suppress the concentration quenching and even enhance the fluorescence emission in the solid state.

Aiming at the organic-crystal laser of high performance in this work, we have designed and synthesized a novel class of ESIPT materials, hydroxy-substituted tetraphenyl imidazole (HPI) and its acetate-containing derivative, HPI-Ac (see Scheme 2), which readily form strongly fluorescent large single crystals with proper intermolecular stacking. It was initially considered that the four phenyl rings in HPI and HPI-Ac would favorably reduce the intermolecular vibronic interactions which would otherwise induce the nonradiative deactivation process.[14] In this paper, we report on the crystal structure, photoluminescence, and amplified spontaneous emission (ASE) of HPI and HPI-Ac.

Experimental Section

Benzil, salicylaldehyde, aniline, 4-aminophenylethyl alcohol, and ammonium acetate were purchased from Aldrich. Glacial acetic acid was obtained from J. T. Baker. All reagents were used as received. Chemical structures were fully identified by ^{1}H NMR (JEOL, JNM-LA300), GC-MS (JEOL, JMS-AX505WA), and elemental analysis (CE Instrument, EA1110).

Synthesis of Hydroxy-Substituted Tetraphenyl Imidazole (HPI), 2-(1,4,5-Triphenyl-1*H*-imidazol-2-yl)phenol. A 5.0 g amount of benzil (23.8 mmol) and 2.55 mL of salicylaldehyde (23.8 mmol) were dissolved in 120 mL of glacial acetic acid at room temperature. A 3.25 mL amount of aniline (35.7 mmol) was added dropwise to this solution, and 9.17 g of ammonium acetate (119 mmol) was added subsequently. The mixture was heated at 110 °C for 12 h. After the termination of reaction, the dark solution was poured into a copious amount of water. Recrystallization from an ethyl acetate solution afforded 6.50 g of white HPI powder with a 72% overall yield. HPI, mp 254 °C; ^{1}H NMR (300 MHz, $CDCl_3$) δ [ppm] 6.46 (t, 1H), 6.54 (d, 1H), 7.08 (d, 1H), 7.12−7.41 (m, 14H), 7.55 (d, 2H), 13.48 (s, 1H); MS (EI) calcd for $C_{27}H_{20}N_2O$ 388.16, found 388. Anal. Calcd for $C_{27}H_{20}N_2O$: C, 83.48; H, 5.19; N, 7.21. Found: C, 83.37; H, 5.19; N, 7.19.

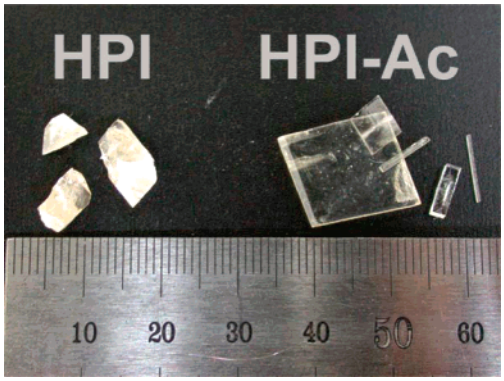

Figure 1. Photograph showing single crystals of HPI and HPI-Ac (ruler scale is in millimeter units).

Synthesis of Acetyloxyethyl-Substituted HPI (HPI-Ac), Acetic Acid 2-{4-[2-(2-Hydroxyphenyl)-4,5-diphenylimidazol-1-yl]phenyl}-ethyl Ester. A 5.0 g amount of benzil (23.8 mmol) and 2.55 mL of salicylaldehyde (23.8 mmol) were dissolved in 120 mL of glacial acetic acid at room temperature. A 4.89 g amount of 2-(4-aminophenyl)ethanol (35.7 mmol) and 9.17 g of ammonium acetate (119 mmol) were added subsequently. The mixture was heated at 110 °C for 12 h. After the termination of reaction, the dark solution was poured into a copious amount of water. Recrystallization from an ethyl acetate solution afforded 7.9 g of white HPI-Ac powder with a 70% overall yield. Transparent and large single crystals, one dimension of which was at least over 1 cm (Figure 1b), were readily obtained within a couple of weeks by the slow evaporation of the ethyl acetate solution of HPI-Ac. HPI-Ac, mp 164 °C; ^{1}H NMR (300 MHz, $CDCl_3$) δ [ppm] 2.00 (s, 3H), 2.95 (t, 2H), 4.28 (t, 2H), 6.46 (t, 1H), 6.54 (d, 1H), 7.05−7.28 (m, 14H), 7.51−7.55 (m, 2H), 13.46 (s, 1H); MS (EI) calcd for $C_{31}H_{26}N_2O_3$ 474.19, found 474). Anal. Calcd for $C_{31}H_{26}N_2O_3$: C, 78.46; H, 5.52; N, 5.90. Found: C, 78.24; H, 5.53; N, 5.87.

Synthesis of Methyl-Blocked HPI Derivative, 2-(2-Methoxyphenyl)-1,4,5-triphenyl-1*H*-imidazole (MeOPI). A 1.5 g amount of HPI (3.86 mmol) was dissolved in *N*,*N*′-dimethylformamide (DMF) at room temperature. A 1.07 g amount of K_2CO_3 (7.72 mmol) and 0.48 mL of iodomethane (7.72 mmol) were added sequentially, and then the mixture was stirred under dark conditions for 12 h. After purification, 1.55 g of white MeOPI powder was obtained quantitatively. MeOPI, mp 208 °C; ^{1}H NMR (300 MHz, $CDCl_3$) δ [ppm] 3.31 (s, 3H), 6.68 (d, 1H), 6.88−6.91 (m, 2H), 7.00 (t, 1H), 7.09−7.34 (m, 12H), 7.60 (d, 2H), 7.65 (d, 1H); MS (EI) calcd for $C_{28}H_{22}N_2O$ 402.17, found 402. Anal. Calcd for $C_{28}H_{22}N_2O$: C, 83.56; H, 5.51; N, 6.96. Found: C, 83.32; H, 5.61; N, 6.96.

Measurements. CW absorption and emission/excitation spectra were obtained by using a UV/vis spectrometer (Scinco, S-3100) and a fluorimeter consisting of a 75-W Xe lamp (Acton Research, XS432) and two monochromators (Acton Research, Spectrapro-150 and -300), respectively. Photoluminescence quantum efficiencies (Φ_{PL}) for solutions were obtained using 9,10-diphenylanthracene as a reference.[15] On the other hand, Φ_{PL} of the crystal was measured using a 6-in. integrating sphere (Labsphere, 3P-GPS-060-SF) equipped with a 325-nm CW He−Cd laser (Omnichrome, Series 56) and a PMT detector (Hamamatsu, PD471) attached to a monochromator (Acton Research, Spectrapro-300i). The detailed analytical procedure to obtain solid-state crystal Φ_{PL} has been described elsewhere.[16] Fluorescence kinetic profiles were measured by using an actively/passively mode-locked Nd:YAG laser

(11) Kim, S.; Park, S. Y.; Yoshida, I.; Kawai, H.; Nagamura, T. *J. Phys. Chem. B* **2002**, *106*, 9291.
(12) Kim, S.; Park, S. Y.; Kawai, H.; Nagamura, T. *Macromolecules* **2002**, *35*, 2748.
(13) (a) An, B.-K.; Kwon, S.-K.; Jung, S.-D.; Park, S. Y. *J. Am. Chem. Soc.* **2002,** *124*, 14410. (b) An, B.-K.; Lee, D.-S.; Lee, J.-S.; Park, Y.-S.; Song, H.-S.; Park, S. Y. *J. Am. Chem. Soc.* **2004,** *126*, 10232.
(14) (a) Birks, J. B. *Photophysics of Aromatic Molecules*; Wiley: London, 1970. (b) Cornil, J.; Beljonne, D.; Calbert, J.-P.; Brédas, J.-L. *Adv. Mater.* **2001**, *13*, 1053.
(15) Berlman, I. B. *Handbook of Fluorescence Spectra of Aromatic Molecules*; Academic Press: New York, 1971.
(16) de Mello, J. C.; Wittmann, H. F.; Friend, R. H. *Adv. Mater.* **1997**, *9*, 230.

(Quantel, YG701) and a 10-ps streak camera (Hamamatsu, C2830) attached to a CCD detector (Princeton Instruments, RTE128H) as an excitation source and a detector, respectively. Samples were excited at right angles by pulses of 355 nm, the third-harmonic pulses of the laser, or at the front face by pulses of 315 nm, generated through a Raman shifter filled with methane at 10 atm and pumped by the fourth-harmonic pulses (266 nm) of the laser. Emission wavelengths were selected by combining band-pass and cutoff filters. Fluorescence kinetic parameters were extracted by fitting measured kinetic profiles to the computer-simulated exponential curves convoluted with instrumental response functions (IRF $\approx$ 25 ps). Pulse-excited emission spectra were measured at a right angle to the excitation (355 nm) with an intensified CCD (Princeton Instruments, ICCD576G) attached to a spectrometer (Acton Research, Spectrapro-500).

Results and Discussion

Both HPI and HPI-Ac were readily synthesized according to the classical method of lophine synthesis in good yields (see Scheme 2).[17] In the synthesis of HPI-Ac, acetyl-blocking of the aliphatic alcohol group was automatically effected due to the reactivity of glacial acetic acid used as the reaction medium. Large single crystals of HPI and HPI-Ac were easily grown from dilute solutions, both of which belong to the triclinic system and $P\bar{1}$ space group (vide infra). Particularly, HPI-Ac tended to form transparent, clear, and well-defined fluorescent single crystals, as large as 20 mm $\times$ 25 mm $\times$ 5 mm (see Figure 1). When observed under a crossed Nicols configuration of the polarizer and analyzer, bright and dark images of the crystals were strictly switched at each 45° rotation, suggesting that the morphology of the crystals are not polycrystalline.[18] Single crystals are free of grain boundary defects, in contrast to conventional solution-processed thin films. Therefore, high-quality single crystals with strong fluorescence emission are important research targets for the fabrication of organic diode lasers. However, only a few investigations have been reported so far on the fluorescence emission and ASE from single crystals because of the difficulty in obtaining large single crystals showing efficient luminescent properties.[18,19]

In the design of the HPI molecule, four phenyl groups were deliberately incorporated into the central imidazole unit to adjust the intermolecular interactions, considering that the molecular packing modes strongly affect the solid-state photoluminescence. The incorporation of steric groups on the chromophore can improve the emission properties by limiting the excessively tight stacking and consequent intermolecular vibronic relaxation. Among the four phenyl rings, two of them, at 2- and 4-positions of imidazole, are responsible for the ESIPT activity and the other two are intended to provide a steric restriction between molecules. These structural characteristics of the HPI molecule could be well revealed by semiempirical calculations and the X-ray crystallographic analysis (Figure 2). The crystal data of HPI and HPI-Ac are summarized here. HPI: $C_{27}H_{20}N_2O$, M = 388.46, triclinic, a = 10.442(2) Å, b = 10.423(2) Å, c = 18.967(4) Å, α = 91.734(4)°, β = 97.363(4)°, γ = 91.588(4)°, V = 2045.4(8) Å^3, T = 233(2) K, space group $P\bar{1}$ (No. 2), Z = 4, μ(Mo Kα) = 0.529 mm^{-1}, 10 461 reflections measured, 8437 unique (R_{int} = 0.0159) which were used in all calculation, R_1 = 0.1082, wR_2 = 0.1690 [$I > 2\sigma(I)$] and R_1 = 0.1681, wR_2 = 0.1888 for all data. HPI-Ac: $C_{31}H_{26}N_2O_3$, M = 474.55, triclinic, a = 9.7716(15) Å, b = 10.2228(16) Å, c = 12.723(2) Å, α = 91.335(3)°, β = 98.148(3)°, γ = 91.295(3)°, V = 1257.4(3) Å^3, T = 233(2) K, space group $P\bar{1}$ (No. 2), Z = 2, μ(Mo Kα) = 0.547 mm^{-1}, 7973 reflections measured, 5769 unique (R_{int} = 0.0260) which were used in all calculations, R_1 = 0.0621, wR_2 = 0.1316 [$I > 2\sigma(I)$] and R_1 = 0.1826, wR_2 = 0.1801 for all data.

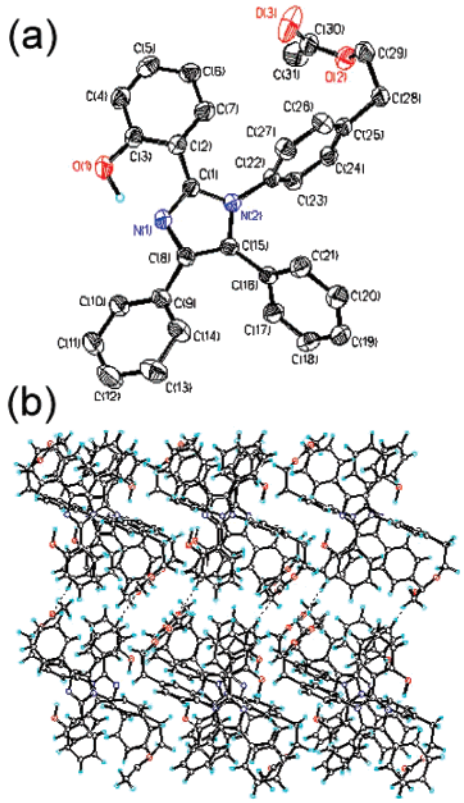

Figure 2. (a) ORTEP drawing of HPI-Ac; for clarity, hydrogen atoms were omitted except the ESIPT-active area. (b) Molecular packing diagram of HPI-Ac in a crystal.

Semiempirical calculations on the isolated system were carried out using PM3 parameters in the MOPAC97 programs (Fujitsu). The optimized geometries of HPI and HPI-Ac gave H-bonded planar conformations comprising central imidazole and two phenyl rings, at the 2- and 4-positions, while the other phenyl rings, at the 1- and 5-positions, were severely distorted, up to 87° out of the plane of imidazole. This was again evidenced by the X-ray analysis, showing that the crystal structures of HPI and HPI-Ac are triclinic and the two phenyl rings at the 1- and 5-positions of the central imidazole ring are twisted almost perpendicular to the chromophore plane. It is presumed that these two twisted phenyl rings are appropriately preventing direct stacking of the active chromophores in a zigzag manner and maintaining proper intermolecular distances, suppressing the concentration quenching of fluorescence, and thus keeping the single crystals strongly fluorescent (Figure 5b).[14] The fluorescence quantum efficiencies (Φ_{PL}) of HPI and HPI-Ac in $CHCl_3$ solutions were both measured to be 0.18. On the other hand, Φ_{PL} of HPI-Ac crystal was measured to be 0.32, indicating the enhanced fluorescence emission due to the reduced intermolecular interaction in the crystalline state.

(17) Radziszewski, B. *Chem. Ber.* **1877**, *10*, 70.
(18) Ichikawa, M.; Hibino, R.; Inoue, M.; Haritani, T.; Hotta, S.; Koyama, T.; Taniguchi, Y. *Adv. Mater.* **2003**, *15*, 213.
(19) Zhu, X.; Gindre, D.; Mercier, N.; Frère, P.; Nunzi, J.-M. *Adv. Mater.* **2003**, *15*, 906.

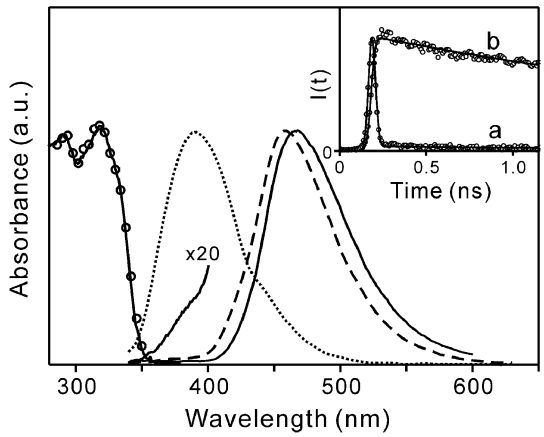

Figure 3. Absorption and emission (excitation at 318 nm) spectra of HPI-Ac (solid) and MeOPI (dotted) in $CHCl_3$ (1.0×10^{-5} M) and a single crystal of HPI-Ac (dashed) at room temperature. The excitation spectrum, monitored at 530 nm, of the HPI-Ac solution (circles) is also depicted. Inset: Fluorescence kinetics of crystalline HPI-Ac, excited at 315 nm (1 μJ cm^{-2} s^{-1}) and monitored at 380 nm (a) and 530 nm (b).

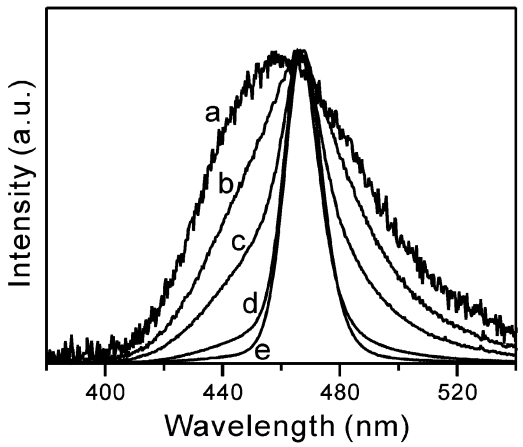

Figure 4. Peak-normalized emission spectra of a single crystal of HPI-Ac at various pulse excitation energies: (a) 0.11, (b) 0.38, (c) 0.49, (d) 0.79, and (e) 3.5 mJ cm^{-2} pulse^{-1}.

Figure 3 shows the absorption and emission spectra of HPI-Ac in $CHCl_3$. Upon $S_0 \rightarrow S_1$ ($\pi\pi^*$) excitation ($\lambda_{max} = 318$ nm, $\epsilon_{318} = 1.0 \times 10^5$ M^{-1} cm^{-1}), a strong fluorescence at 465 nm and a shoulder-like very weak one at around 390 nm were observed. The excitation spectra, monitored at the respective bands, are identical and spectrally the same as the lowest absorption band, indicating that both fluorescence bands originate from the same ground-state species. In comparison, MeOPI, a non-proton-transfer model compound which lacks a hydroxyl proton, shows only a normal Stokes-shifted fluorescence at 389 nm. Therefore, we could unambiguously assign the 390-nm band as the normal E* fluorescence and the 465-nm band as the K*-tautomer fluorescence. Occurrence of ESIPT in HPI and HPI-Ac is also rationalized because the imidazole unit in their structure is a well-known motif for ESIPT.[20,21] Effectively, HPI shows the same spectral behaviors as HPI-Ac. For the optical studies of fluorescent single crystals, the HPI-Ac crystal was selected and investigated intensively due to its higher optical quality and well-defined planar shape. Upon absorption of a photon, crystalline HPI-Ac exhibited strong K*-tautomer fluorescence at 458 nm, hypsochromically shifted about 330 cm^{-1} with respect to that of the dilute HPI-Ac solution. This is possibly attributed to the geometric restriction in its crystalline state. The fluorescence at 380 nm of crystalline HPI-Ac shows a biexponential decay composed of a very fast, temporal-resolution-limited component ($\sim$5 ps, 99.9%) and a 4.4-ns (0.1%) component, while the fluorescence at 530 nm rises within our temporal resolution and decays in 4.4 ns, showing a typical ESIPT rate of $\geq$(5 ps)$^{-1}$ (see the inset in Figure 3).[22,23]

When the crystalline HPI-Ac single-crystal sample was excited by a 355-nm picosecond pulse ($\sim$25 ps) of circular excitation area, the blue K* emission was amplified into the intense and narrow blue band. Figure 4 shows the spectral evolution as a function of the pump intensity, where the emission was collected from the edge of the crystal. The diameter of the pump beam was 9 mm, and the intensity was tuned from 0.11 to 3.5 mJ cm^{-2} pulse^{-1} onto the sample without focusing. Even though the spectral narrowing was observed easily with the nonfocused beam, a loss of spectral narrowing was also monitored when the diameter of the pump beam was below a certain size, which is one of the characteristics associated with ASE.[24] The fluorescence emission and ASE of the sample shown in Figure 4 were collected in a direction perpendicular to the excitation beam under the optimized geometry of polarization, as shown in Figure 5a. At a low pump fluence of 0.11 mJ cm^{-2} pulse^{-1}, the emission spectrum was initially very broad and the full width at half-maximum (fwhm) was approximately 67 nm. When the pump fluence was gradually increased, the fwhm decreased to 13 nm in this system. To optimize the gain-narrowing condition, we used a cylindrical lens to form a line focus (500 μm $\times$ 9 mm, Figure 5b) on the front surface of the sample. The polarization direction of the pump was varied with a half-wave plate. The gain-narrowing of HPI-Ac crystal was strongly dependent on the pump polarization, as expected. When the polarization was aligned parallel to the active chain orientation, the gain-narrowing was observed at a lower pump fluence, and the fwhm was also decreased to 9 nm (see Figure S-4 in the Supporting Information).

Figure 6a shows the evolution of the fwhm and the hyperlinear dependency of integrated emission for the HPI-Ac crystal as a function of the pump intensity. It is noted that the emission intensity is approximately proportional to the pump fluence up to 250 μJ cm^{-2} pulse^{-1}, after which the characteristic hyperlinear dependence is clearly developed. The observation that the narrowing of line shape and the hyperlinear dependence occur at the similar pump energy indicates that both effects are the results of light amplification at the wavelength where the single crystal has a high gain. The onset of significant spectral narrowing, which we will call the phenomenological threshold, was determined to be around 200 μJ cm^{-2} pulse^{-1} in the nonfocused state and 6 μJ cm^{-2} pulse^{-1} in the line-focused state, respectively. Above this "threshold", spontaneous emission from one emitter efficiently stimulates emission as it propagates along

(20) Rodríguez, M. C. R.; Penedo, J. C.; Willemse, R. J.; Mosquera, M.; Rodríguez-Prieto, F. *J. Phys. Chem. A* **1999**, *103*, 7236.
(21) Gostev, F. E.; Kol'tsova, L. S.; Petrukhin, A. N.; Titov, A. A.; Shiyonok, A. I.; Zaichenko, N. L.; Marevtsev, V. S.; Sarkisov, O. M. *J. Photochem. Photobiol. A: Chem.* **2003**, *156*, 15.
(22) Chou, P.-T.; Chen, Y.-C.; Yu, W.-S.; Chou, Y.-H.; Wei, C.-Y.; Cheng, Y.-M. *J. Phys. Chem. A* **2001**, *105*, 1731.
(23) Chang, D. W.; Kim, S.; Park, S. Y.; Yu, H.; Jang, D.-J. *Macromolecules* **2000**, *33*, 7223.
(24) Johansson, N.; Salbeck, J.; Bauer, J.; Weissörtel, F.; Bröms, P.; Andersson, A.; Salaneck, W. R. *Adv. Mater.* **1998**, *10*, 1136.

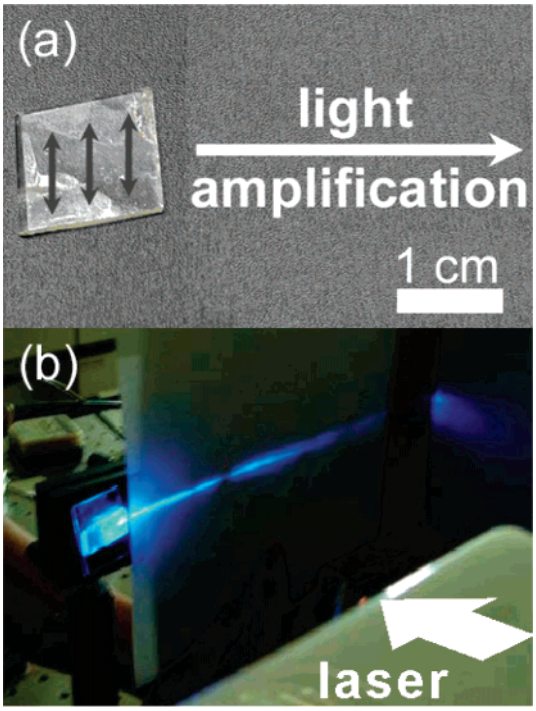

Figure 5. (a) Schematic representation of the optimal polarization direction in the HPI-Ac single crystal. (b) Photograph of a straight path, at a right angle to the photoexcitation, of blue ASE at the excitation fluence of 10 mJ cm^{-2} $pulse^{-1}$. A cylindrical lens was used to shape the photoexcitation beam into a stripe with a width of approximately 500 μm and a length of 9 mm.

the excited region of the sample. Amplification occurs preferentially where the stimulated-emission cross-section is maximum, leading to gain-narrowing. The main mechanism for the observed gain-narrowing is attributed to ASE by the observations of the waveguiding property and the effect of excitation beam shape in light amplification.[11,24−26]

The picosecond kinetics in Figure 6b gives direct evidence of light amplification via an ASE mechanism. The emission profiles show the reduction of lifetime compared with the spontaneous emission (4000 ps); lifetime decreases from 1400 ps (at 37 μJ cm^{-2} $pulse^{-1}$) to 80 ps (at 1900 μJ cm^{-2} $pulse^{-1}$) with increasing excitation energy. The inversely proportional dependence of the decay time on the pump energy is consistent with the excited-state population-depletion model explaining ASE phenomena.[27] The intrinsic four-level nature of ESIPT contributes to the easy population inversion, and thus the phenomenological ASE threshold of HPI-Ac is lower than that of conventional laser dyes.[19,24,28,29] Such low-threshold ASE is a promising property for the application of this crystal as a medium for optical amplifiers or lasers. Moreover, HPI-Ac single crystals have long-term photostability and thermostability when compared with dye-doped polymer films. Although the crystal was repeatedly exposed to 355-nm picosecond pulses (4×10^4 shots), no discernible photobleaching or decomposition was observed under an excitation power of 2 mJ cm^{-2} $pulse^{-1}$.

(25) Yanagi, H.; Morikawa, T. *Appl. Phys. Lett.* **1999**, *75*, 187.
(26) Shaklee, K. L.; Leheny, R. F.; Nahory, R. E. *Phys. Rev. Lett.* **1971**, *26*, 888.
(27) Siegman, A. E. *Lasers*; University Science Books: Mill Valley, CA, 1986.
(28) Hibino, R.; Nagawa, M.; Hotta, S.; Ichikawa, M.; Koyama, T.; Taniguchi, Y. *Adv. Mater.* **2002**, *14*, 119.
(29) Nagawa, M.; Hibino, R.; Hotta, S.; Yanagi, H.; Ichikawa, M.; Koyama, T.; Taniguchi, Y. *Appl. Phys. Lett.* **2002**, *80*, 544.

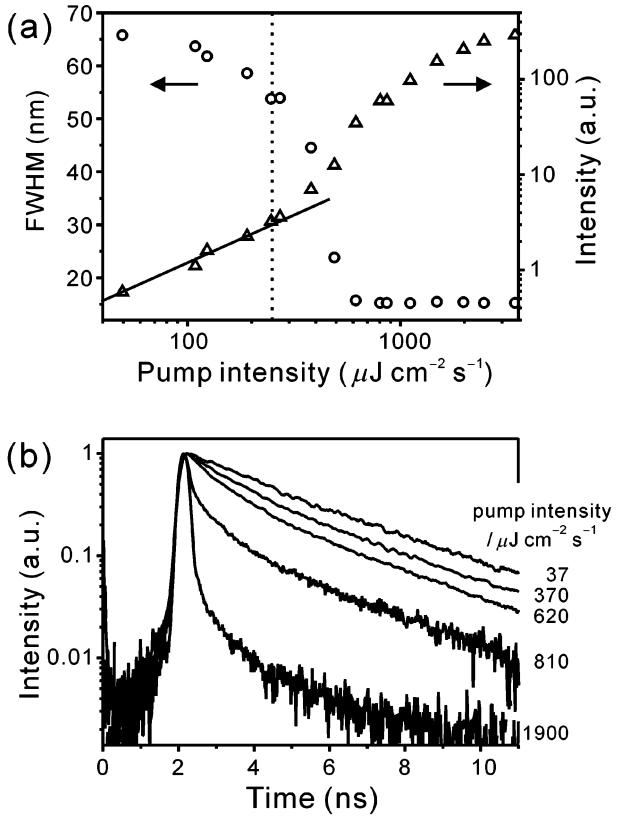

Figure 6. (a) Integrated emission intensity and fwhm of emission spectra, excited by 355-nm pulses of circular area having a diameter of 9 mm, of a single crystal of HPI-Ac as a function of pump energy. A solid line shows slope = 1. A dotted line shows the phenomenological threshold where ASE occurs. (b) Time-resolved fluorescence kinetics, excited at 355 nm and monitored at 530 nm, of a single crystal of HPI-Ac at various pump energies.

In conclusion, the strongly fluorescent large single crystal of a hydroxy-substituted tetraphenylimidazole derivative (HPI-Ac) was successfully synthesized and characterized to show very efficient amplified spontaneous emission (ASE) associated with the excited-state intramolecular proton transfer (ESIPT) process. From the X-ray crystallographic analysis and semiempirical molecular orbital calculation, it was found that the four phenyl groups substituted in the imidazole ring of HPI-Ac provided the positive steric effect toward the improved fluorescence emission by limiting the excessive tight-stacking responsible for the intermolecular vibrational coupling and relevant nonradiative relaxation.

Acknowledgment. This work was supported by the Ministry of Science and Technology of Korea through the National Research Laboratory (NRL) program, awarded to Prof. Soo Young Park. We are grateful for the instrumental support from the equipment facility of CRM-KOSEF, Korea University. D.-J.J. and O.-H.K. thank the Korea Research Foundation for Grant KRF-2004-015-C00230 and the Brain Korea 21 Program, respectively.

Note Added after ASAP Publication. Incorrect bibliographic information was reported in reference (9) of the version published ASAP June 15, 2005. The corrected version was published ASAP June 21, 2005.

Supporting Information Available: Optical characteristics and crystallographic information (PDF, CIF). This material is available free of charge via the Internet at http://pubs.acs.org.

JA0508727